NANO LETTERS

2008
Vol. 8, No. 7
1819-1824

Contact Effects in Graphene Nanoribbon Transistors

Gengchiau Liang,*,† Neophytos Neophytou,‡ Mark S. Lundstrom,‡ and Dmitri E. Nikonov§

Department of Electrical and Computer Engineering, National University of Singapore, Singapore 117576, School of Electrical and Computer Engineering, Purdue University, West Lafayette, Indiana, 47907-1285, and Technology and Manufacturing Group, Intel Corporation, SC1-05, Santa Clara, California 95052

Received January 26, 2008; Revised Manuscript Received April 9, 2008

ABSTRACT

The effects of the various contact types and shapes on the performance of Schottky barrier graphene nanoribbon field-effect-transistors (GNRFETs) have been investigated using a real-space quantum transport simulator based on the NEGF approach self-consistently coupled to a three-dimensional Poisson solver for treating the electrostatics. The device channel considered is a double gate semiconducting armchair nanoribbon. The types of contacts considered are (a) a semi-infinite normal metal, (b) a semi-infinite graphene sheet, (c) finite size rectangular shape armchair graphene contacts, (d) finite size wedge shape graphene contacts, and (e) zigzag graphene nanoribbon contacts. Among these different contact types, the semi-infinite graphene sheet contacts show the worst performance because of their very low density of states around the Dirac point resulting in low transmission possibility through the Schottky barrier, both at ON and OFF states. Although all other types of contacts can have significant enhancement in I_{ON} to I_{OFF} ratio, the zigzag GNR contacts show promising and size invariant performance due to the metallic properties.

Introduction. Recent studies on graphene based materials have attracted a lot of attention from various fields due to their unique electronic and physical properties[1] such as quantum Hall effects,[2,3] extremely high carrier mobility,[1] and so forth, which are able to be employed in different applications.[4–14] Their potential application to field-effect transistors (FETs) grew a large interest from the nanoelectronics device research community in the search of an alternative channel material that might overcome the physical scaling limitations of the Si-based nano MOSFETs and the fabrication challenges of carbon nanotube (CNT) FETs. Recent experimental studies[4,5] indicate the possibility of fabricating graphene nanoribbon (GNR) transistors, and the potential of GNRs as an alternative method to bypass the CNT chirality challenge while still retaining the excellent electronic properties of graphene sheets, such as the high electron/hole mobility (also properties of CNTs). Furthermore, previous theoretical studies using semiclassical[6,7] and quantum transport models[8–11] have shown that GNR MOSFETs could have a similar ON-state current performance as carbon nanotube (CNT) MOSFETs and might outperform traditional Si MOSFETs. In order to achieve high performance, a MOSFET type of device with doped source and drain regions should be realized. However, for a transistor in such nanoscale size, doping a GNR of less than 3 nm width can be an extremely challenging task. Hence, metal contacts to form the Schottky barrier (SB) FETs would be preferred and might be more feasible from fabrication and experimental point of view. Specifically, it is of great interest to make use of the graphene sheet itself as the devices' contacts because of its semimetallic properties. Therefore, the dependence of the device behavior of the GNR FETs on the contact types and shapes of the graphene sheet needs to be investigated properly in order to provide theoretical guidance to experimentalists.

In this work, we implement a full real-space quantum transport simulator using the nonequilibrium Green's function (NEGF) approach[16] self-consistently coupled to a three-dimensional (3D) Poisson solver for treating the electrostatics.[9] A simple π-orbital model[17] with consideration of edge effects[18] is assumed for the device Hamiltonian. Using this model, we evaluate the ballistic performance of double-gate GNR SB FETs with different types and shapes of contacts as shown in Figure 1. We investigate the effect of five different types of contacts, (a) the semi-infinite normal metal with constant surface density of states in the energy region of interest (L and $W \rightarrow \infty$), (b) the semi-infinite graphene sheet contacts (L and $W \rightarrow \infty$), (c) the finite size rectangular graphene type of contacts, (d) the finite size wedge shape contacts, and (e) the one-dimensional (1D) zigzag GNRs

* Corresponding author. E-mail: elelg@nus.edu.sg.
† National University of Singapore.
‡ Purdue University.
§ Intel Corporation.

10.1021/nl080255r CCC: $40.75
Published on Web 06/18/2008

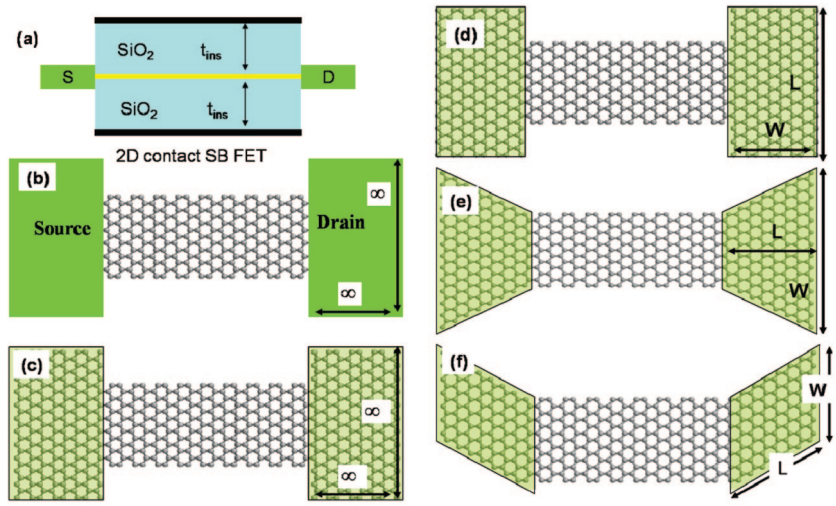

Figure 1. (a) Schematic of the simulated dual-gate graphene nanoribbon SBFETs. The oxide thickness (t_{ins}) is 1 nm and the channel length is 12.5 nm. (b−f) Top view of (a) for different contact shapes. (b) The source and drain parts are composed by a semi-infinite metal (L and W → ∞). (c) The source and drain parts are composed by a semi-infinite graphene (L and W → ∞). (d) The source and drain parts are composed by a finite rectangular shape graphene electrode. (e) The source and drain parts are wedge shaped graphene sheets[15] with zigzag edges. These contacts gradually decrease their width from infinite (far from the channel) to the size of the channel (at the contact points). (f) The GNR contact with zigzag edges and same width as the channel.

contacts. (Note that the nanoribbons are designated as zigzag or armchair by the shape of their edge; it is in a sense opposite to the designation of carbon nanotubes). By keeping the same GNR FET channel width and length, but changing the contacts, we find that the semi-infinite normal metal can potentially provide promising performance,[19] whereas the semi-infinite graphene contacts show the worst performance. The finite-size wedge shape graphene contacts and the finite-size rectangular shape graphene contacts indicate enhanced I_{ON} to I_{OFF} ratios compared with the graphene case contacts. The zigzag GNR contacts, however, due to their strong natural metallic properties, also show promising performance, independent of the contact's length. They could be the candidates for the source/drain materials or even possibly an interconnect material[14] between the metallic electrodes and the channel. Although the intrinsic (undoped) semi-infinite graphene contacts have poor performance, once they are doped (chemically or electrostatically) they exhibit a better performance in terms of I_{ON} to I_{OFF} ratio.

Methodology. A simple π-orbital model which also takes the edge effects into consideration as described in ref 18 is used for the device Hamiltonian. Calculation of the bandgap of the nanoribbon using a simple π-orbital approach without considering the edge effects indicates two different type of ribbons, semiconducting (finite bandgap) and metallic (zero bandgap). This is very similar to the case of zigzag carbon nanotubes (CNTs), where there are two different ribbon types, metallic and semiconducting. In the case of the semiconducting ribbons, the bandgap is a monotonically decreasing function of the GNR width. When considering edge effects (by varying the hopping parameters of the edge atoms[18]), however, the calculated bandgap is always finite and three different groups, that follow three different envelope functions, can be identified. Since the bandgap is finite, all three of these groups have semiconducting behavior. The reason for this behavior is attributed to the different amount of charge that accumulates on the edges in each case.[18] In order to capture this unusual behavior, in this work, the edge effect is included in the channel edge as well as in the contacts' edges of the simulated devices.

We utilize a full real-space quantum transport simulator based on the nonequilibrium Green's function (NEGF) approach[16] self-consistently coupled to a 3D Poisson's equation solver for treating the electrostatics. We then investigate the impact of the contact type and shape on the GNR FETs ballistic current−voltage characteristics. The NEGF equations can be briefly summarized as:

$$G(E) = [(E + i0^+)I - H_D - \Sigma_S - \Sigma_D]^{-1}$$

$$G^n(E) = G\Sigma^{in}G^+$$

$$\rho_j = e\int_{-\infty}^{\infty} \frac{dE}{2\pi} G_j^n(E) \quad \text{and}$$

$$I_{j\to j+1} = \frac{ie}{\hbar}\int_{-\infty}^{\infty} \frac{dE}{2\pi}[H_{D,j,j+1}G^n_{j+1,j}(E) - H_{D,j+1,j}G^n_{j,j+1}(E)] \qquad (1)$$

where H_D is the device Hamiltonian using a π-orbital nearest-neighbor tight binding model with edge effect modification and Σ_S and Σ_D are the self-energies for the left (source) and right (drain) reservoirs. In general,

$$\Sigma_{S,D} = \tau_{S,D} \times g^S_{S,D} \times \tau^+_{S,D}$$

where $\tau_{S,D}$ is the interaction between the device and the contacts and $g^S_{S,D}$ are the surface Green's function of the contacts. On the basis of the different geometry and type of the contacts, the self-energy can capture their physical properties. For example, when the semi-infinite normal metal is assumed, $g^S_{S,D}$ is calculated using a phenomenological model[19,20] to obtain constant density of states for the normal metal and to get the broadening around 0.2 eV in the interesting bias window. However, when graphene materials are assumed for the contacts, the self-energy has to capture the graphene sheet properties precisely for the different shapes. For example, the semimetallic density of states of

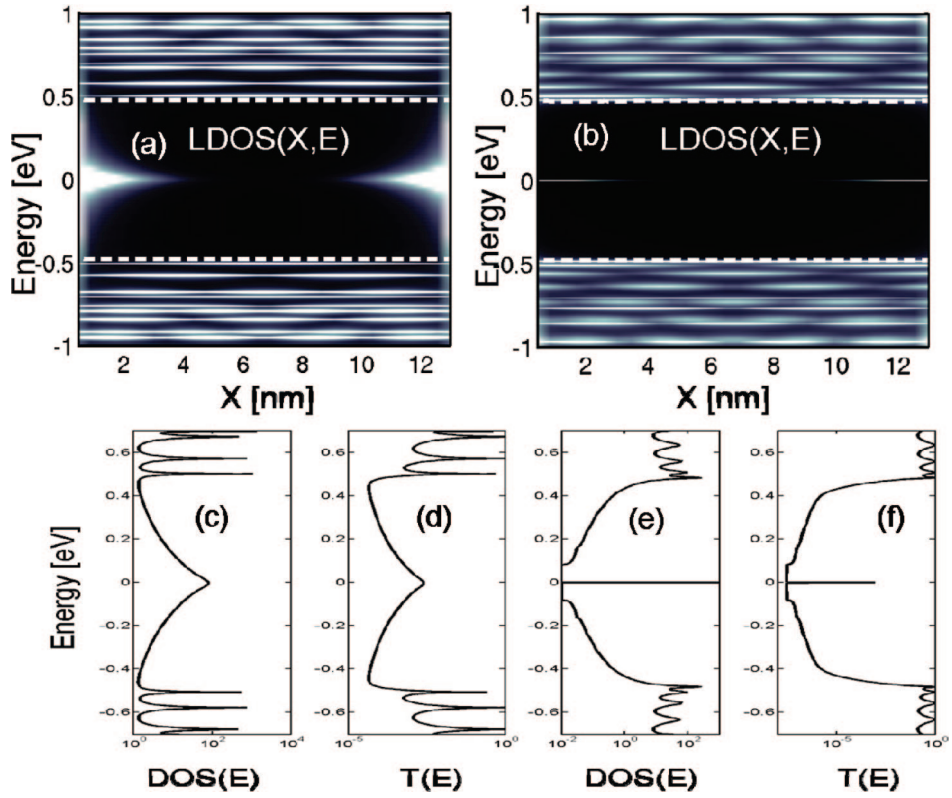

Figure 2. (a,b) The local density of states, LDOS(x,E), of armchair GNR SBFET with (a) semi-infinite normal metal and (b) semi-infinite graphene sheet type of contacts. The channel GNR is 1.6 nm wide and 12.5 nm long. (c,d) The total density of states, DOS(E), and transmission T(E) for case (a). A wide peak appears at the middle of the bandgap because of the constant DOS(E) in the metal contact near the Fermi point. (e,f) The total density of states, DOS(E), and transmission T(E) for case (b). A sharp peak appears at the middle of the bandgap because of zero DOS graphene sheet contact near the Fermi point.

the graphene sheet can be calculated using the proper self-energy of the semi-infinite graphene sheets.[9] We would like to emphasize here that it is only a simplified model for generic metal electrodes. It ignores the complicated band structure of the metal and does not capture the differences of carrier transport in the GNR with various metals as contacts.[21] It is used here only to contrast the behavior of a typical metal and graphene, which is a semimetal and has a vanishing density of states at the Dirac point.

Results and Discussions. Figure 2a,b shows the local density of states at equilibrium *LDOS(X, E)*,[22] for the first two contact cases, the semi-infinite normal metal and the semi-infinite graphene sheet. Metal induced gap states (MIGS) appear inside the bandgap, near its middle, of the armchair GNRs. These states are mainly localized at the interface between the contacts and the channel, and evanesce from the interface to the center for both cases.

In the semi-infinite normal metal case, MIGS are broadened in energy. The reason for the broadening is the coupling to the states of the metal contact; the DOS(E) of the metal being large and approximately constant close to the middle of the gap. On the other hand, the MIGS in the semi-infinite graphene sheet contact case have a very sharp and narrow peak at the Dirac point and are small elsewhere. The reason for the sharpness of the peak arises from the DOS(E) of the intrinsic graphene sheet which is zero at the Dirac point (midgap) and increases as the energy deviates from that point. This small density of states leads to small broadening of the MIGS peak. Other than the Dirac point, DOS(E) and $T(E)$ are suppressed at all other energies in the bandgap. Figure 2c shows the integrated DOS(E) over the length of the entire device for the case of the semi-infinite normal metal. The peak of the DOS(E) has a Lorentzian-like broadening caused by the normal metal contacts with the constant density of states. This DOS(E) behavior reflectes in the $T(E)$ of the device (shown in Figure 2d). Figure 2e,f illustrates the sharp peaks in DOS(E) and $T(E)$ for the graphene contact case. These differences between these two contacts will also reflect in the device performance using these two as the contacts.

Figure 3a shows the transfer characteristics of GNR FETs of different widths (1.4, 1.6, 3, and 4 nm) connected to semi-infinite normal metal contacts. Their GNR bandgaps are E_G = 0.66, 0.95, 0.5, and 0.25 eV, respectively. As the bandgap decreases, the performance of GNR devices, in terms of the ratio of I_{ON} to I_{OFF}, degrades. A narrow bandgap favors tunneling, which is the main degradation factor of the I_{ON} to I_{OFF} ratio.[23] Unlike CNT FETs and semiconducting nanowire FETs, the bandgap of armchair GNRs is not a simple monotonically increasing function as the size of the channel decreases. Therefore, narrowing down the width of GNR transistors does not result in a monotonic enhancement in the performance in terms of I_{ON} to I_{OFF} ratio; for example, the 1.6 nm ribbon (dashed line) has better performance than the 1.4 nm ribbon (solid line). This large deviation in the

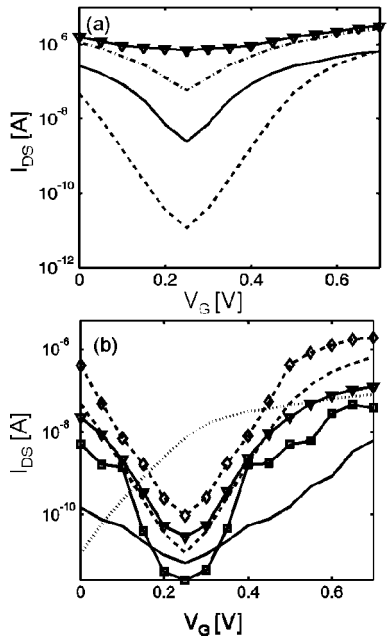

Figure 3. (a) Transfer characteristics of the armchair GNR SBFET with widths of 1.4 nm (solid), 1.6 nm (dashed), 3 nm (dot-dashed), and 4 nm (triangle) under $V_{DS} = 0.5$ V. The contact in all cases is a semi-infinite normal metal. The bandgaps for these different width armchair GNRs are around 0.66, 0.95, 0.5, and 0.26 eV respectively. The 1.6 nm wide armchair GNR FET shows the best I_{ON}/I_{OFF} ratio compared with the other three types because it has the largest bandgap. (b) Transfer characteristics of the 1.6 nm wide GNR SBFET with different types of graphene type of contacts: the semi-infinite normal metal (dashed line), the semi-infinite graphene sheet (solid line, intrinsic (undoped) and dot-dashed line, doped), finite size rectangular shape graphene sheet ($L = 3$ nm, $W = 5$ nm as in Figure 1d; square markers), wedge shape graphene sheet ($L = 3$ nm, $W = 5$ nm as in Figure 1e, triangle markers), and zigzag GNR contacts ($L = 3$ nm, $W = 1.6$ nm as in Figure 1f, diamond markers). The ON (I_{max}) to OFF (I_{min}) ratio are 1.5×10^5, 4×10^3, 1×10^4, 3×10^4, 5×10^3, and 3×10^4 for the contact cases: normal metal, intrinsic graphene sheet, doped graphene sheet, rectangle shape graphene sheet, the wedge shape graphene sheet, and the 1D armchair GNR, respectively. $V_{DS} = 0.5$ V is applied in the simulations.

performance with small deviations in the ribbons' width indicates that one has to precisely control the GNR width in the device fabrication process in order to obtain uniform device performance. We next concentrate on the 1.6 nm width GNR transistor which indicates the best performance, and we examine the effect of different types of contacts (Figure 3b). First, we compare the effect of the semi-infinite intrinsic graphene sheet contacts (solid line) to the semi-infinite normal metal contact case of the previous paragraph (dashed). It is evident that the performance in terms of I_{ON} to I_{OFF} ratio is degraded in the semi-infinite graphene case compared with the semi-infinite normal metal case. The reason of the performance degradation in this case can be attributed to the unique density of states DOS(E) of the graphene sheet, which is very small in energies around the Dirac point (except the peak associated with the midgap states). In this case of a Schottky barrier device, the total currents are mainly dominated by the quantum tunneling current instead of the thermionic current. (The barrier used here is 0.5 eV). Therefore, the current is suppressed in the semi-infinite graphene contact case because of the low density of states and hence low tunneling probability.

Next, we focus on various graphene contacts and examine the device behavior for different shapes of graphene sheet contacts such as the finite size rectangular armchair-edge contact with $L = 3$ nm/$W = 5$ nm (Figure 3b square line), the finite size wedge shape contacts with $L = 3$ nm/$W = 5$ nm (Figure 3b triangle line), and the zigzag GNR contacts with $L = 3$ nm/$W = 1.6$ nm (Figure 3b diamond line) as shown in Figure 1d−f. Compared with the semi-infinite graphene sheet contacts (solid line), we found that all of these different shape contacts enhance the I_{ON}/I_{OFF} ratio, with the finite size rectangular shape contacts providing the best performance among all cases.

To further understand the impact of the contacts on the device performance, in Figure 4a−c, we plot the local density of states LDOS(E) of the devices with semi-infinite graphene type contacts (dashed line), and the normal metal contacts (solid line) at the source-device interface ($x = 0$), the center of the channel, and the drain-device ($x = L_{channel}$) interface, respectively. We consider the ON-state case, with biases $V_{DS} = 0.5$ V and $V_{GS} = 0.6$ V. Although, within the current conducting energy window ($\mu_1 = 0$ and $\mu_2 = -0.5$ eV) the two devices have similar LDOS(E) in the middle of the channel (Figure 4b), there are significant differences in the LDOS(E) at the ends of the devices. The main reason of this difference is the unique nature of the graphene sheets, which have a very low density of states near the midgap level. Therefore, electron transport through this energy region has low transmission probability as shown in Figure 4d. In this case, the transmission of the device with semi-infinite graphene sheet contacts is orders of magnitudes lower than the transmission of the device with semi-infinite normal metal contacts. However, properly engineering the Fermi level of the graphene sheet by adjusting the barrier height, in order to include the high DOS(E) part of graphene energy spectrum in transport, could be helpful to enhance the device performance. For example, if the Fermi level of the graphene is adjusted to be 0.2 eV higher than the intrinsic level (usually achieved by chemical or electrostatic doping,[24–27] the transfer characteristic shows an enhancement of the I_{ON} to I_{OFF} ratio (Figure 3b, dot-dashed line). Furthermore, the performance of SBFET with semi-infinite normal metal contacts strongly depends on the interface between the metal and the GNR,[19,20] and it can be optimized by controlling the barrier height.[19,20,26,27] However, the optimization of device performance is out of the scope of this work. We would like to focus on dependence of the different types of the contacts on the performance of the devices. The effect of the contacts is primarily the distinct DOS(E) that each contact provides to the channel.

To understand the behavior of the devices with the finite size rectangular contacts and the device with the finite size wedge shape contact of Figure 3b, in Figure 4e, we plot the T(E) of the two devices at OFF-state conditions ($V_{GS} = 0.25$ V and $V_{DS} = 0.5$ V). The device with finite size rectangular shape contacts (dashed line), whose bandgap is 50 meV, has a low transmission coefficient inside the bandgap as shown

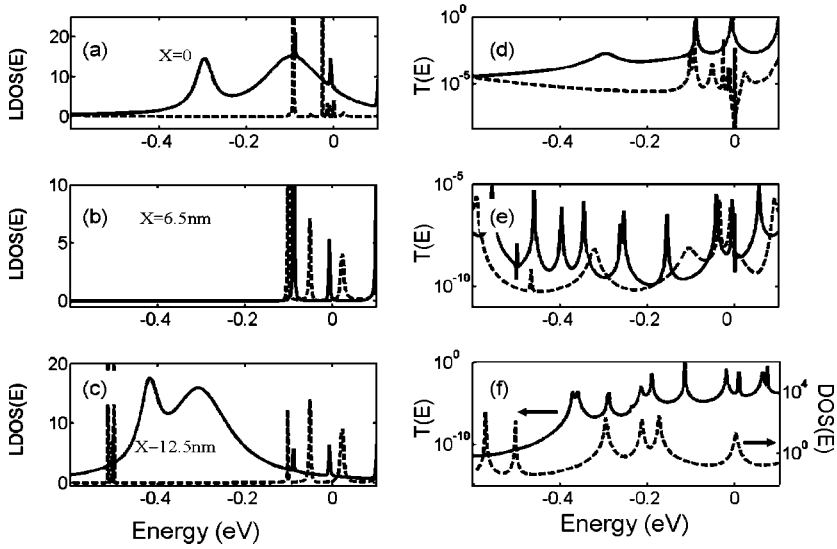

Figure 4. Local density of state vs energy, LDOS(E), of a 12.5 nm channel long and 1.6 nm wide GNR SBFET for the cases of the normal semi-infinite metal contacts (solid) and the case of the intrinsic (undoped) semi-infinite graphene sheet (dashed line) contacts under ON-state conditions, ($V_{GS} = 0.6$ V and $V_{DS} = 0.5$ V) at different places along the length of the channel. (a) at $x = 0$ nm (source), (b) at 6.5 nm (middle of channel), and (c) at 12.5 nm (drain) (d) Transmission vs energy, T(E) for the two devices described. Because of the nature of the graphene sheet, the transmission of the device with semi-infinite graphene sheet contacts is significantly small near the intrinsic level and in the entire $E_{fs}-E_{fd}$ window compared with the semi-infinite metal contact case. (e) The T(E) of the same GNR SBFET with two other type of contacts, the finite size rectangular shape graphene contacts (dashed) and the finite size wedged shape graphene contacts (solid) at OFF-state ($V_{GS} = 0.25$ V and $V_{DS} = 0.5$ V). The oscillation peaks in T(E) of the wedge shape graphene contacts have also been observed in experimental measurements.[28] (f) T(E) at $V_{GS} = 0.7$ V and $V_{DS} = 0.5$ V and DOS(E) under equilibrium of the same GNR FET with zigzag edged contacts.

in Figure 4e, because of the small bandgap and the shape mismatch between the large width armchair GNR contacts and the small width armchair GNR channel. This results in reduction of the OFF-state currents as indicated in Figure 3b (square line). On the other hand, the device with the zigzag edge wedge-shape contact has the worst I_{ON}/I_{OFF} ratio among these three devices because it has a larger transmission probability in the bandgap region and an increased OFF-state current, especially through the contribution of quantum tunneling currents. The reason of this larger transmission in the OFF-state is due to the shape of the contacts which gradually narrows down from a large width to a small one equal to that of the channel and keeps partly metallic properties of the electrodes. Although these two type of contacts result in some device performance improvement over the semi-infinite graphene contact case, the obtained I_{ON}/I_{OFF} ratio is a strong function of their sizes (L and W). When L and W are very large, these two graphene type contacts will have the intrinsic graphene sheet properties and hence a degraded device performance as in the limit of the infinite graphene sheet of Figure 4b (solid).

The zigzag GNR contacts (Figure 1f) exhibit a performance enhancement compared to the case of the rectangular shape graphene contacts. Moreover, the I_{ON}/I_{OFF} ratio remains the same when the length of the contact increases. This is because the zigzag GNRs are materials with metallic properties[6,14] unlike the semi-infinite graphene sheet. Therefore, it can behave similarly to the normal metal contact case with increased DOS(E) and T(E) in the conduction region (Figure 4f), and result in a better device performance in terms of I_{ON} to I_{OFF} ratio.

Conclusion. In summary, the device performance of armchair GNR SBFETs with different channel widths and different type and shape of contacts is investigated theoretically using a real-space quantum transport model based on the NEGF method, self-consistently coupled to a 3D Poisson's solver for treating the electrostatics. The Hamiltonians of the devices and the graphene contacts are described in the π-orbital tight-binding approach with edge effect modification included. We found that, unlike CNT and semiconductor nanowire FETs, decreasing the width of the channel does not always result in I_{ON} to I_{OFF} ratio increase because the bandgap of GNR is not monotonically increasing as the width of the GNR decreases. The effect of different contacts and contact shapes is investigated. Among these different contact types (normal metal and intrinsic semi-infinite graphene sheet) and different shapes of graphene sheet (rectangular shape, wedge shape, and zigzag GNRs), the normal metal contact might be still the best choice for FET-like devices in terms of high I_{ON} to I_{OFF} ratio if the contact properties can be optimized. Out of the graphene contact types, the doped graphene sheet, the undoped rectangle-shape graphene contacts, the undoped wedge shape graphene contacts, and the zigzag GNR could still result in adequate I_{ON} to I_{OFF} ratio, but the zigzag GNR contacts would be the best candidate for a contact because of its metallic properties and the independence of its properties on its length.

Acknowledgment. The work at National University of Singapore was supported by MOE under Grants R-263-000-416-112 and R-263-000-416-133. The work at Purdue

University was supported by the Semiconductor Research Corporation (SRC). G.C. Liang thanks Mr. Kaitak Lam for his help in generating Figure 1. The authors would like to thank the National Science Foundation's Network for Computational Nanotechnology (NCN) for providing computational support through nanoHUB.org.

References

(1) Geim, A. K.; Novoselov, K. S. *Nat. Mater.* **2007**, *6*, 183.
(2) Novoselov, K. S.; Geim, A. K.; Morozov, S. V.; Jiang, D.; Katsnelson, M. I.; Grigorieva, I. V.; Dubonos, S. V.; Firsov, A. A. *Nature* **2005**, *438*, 197.
(3) Zhang, Y.; Tan, Y.; Stormer, H. L.; Kim, P. *Nature* **2005**, *438*, 201.
(4) Berger, C.; Song, Z.; Li, X.; Wu, X.; Brown, N.; Naud, C.; Mayou, D.; Li, T.; Hass, J.; Marchenkov, A. N.; Conrad, E. H.; First, P. N.; de Heer, W. A. *Science* **2006**, *312*, 1191. Li, X.; Wang, X.; Zhang, L.; Lee, S.; Dai, H. *Science* **2008**, *319*, 1229.
(5) Lemme, M. C.; Echtermeyer, T. J.; Baus, M.; Kurz, H. *IEEE Electronic Device Letters* **2007**, *28* (4), 282.
(6) Liang, G.-C.; Neophytou, N.; Nikonov, D. E.; Lundstrom, M. S. *IEEE Trans. Electron Devices* **2007**, *54* (4), 677. Liang, G.-C.; Neophytou, N.; Lundstrom, M. S.; Nikonov, D. E. *Proceedings NSTI Nanotech* 2007, Santa Clara, May 20–24, 2007: pp 127–130.
(7) Ouyang, Y.; Yoon, Y.; Fodor, J. K.; Guo, J. *Appl. Phys. Lett.* **2006**, *89*, 203107.
(8) Yan, Q.; Huang, B.; Yu, J.; Zheng, F.; Zang, J.; Wu, J.; Gu, B.-L.; Liu, F.; Duan, W. *Nano Lett.* **2007**, *7*, 1469.
(9) Liang, G.-C.; Neophytos, N.; Lundstrom, M.; Nikonov, D. *J. Appl. Phys.* **2007**, *102*, 054307.
(10) Ouyang, Y.; Yoon, Y.; Guo, J. *IEEE Trans. Electron Devices* **2007**, *54* (9), 2223.
(11) Fiori, G.; Iannaccone, G. *IEEE Electron Device Lett.* **2007**, *28*, 760.
(12) Wang, Z. F.; Shi, Q. W.; Li, Q.; Wang, X.; Hou, J. G.; Zheng, H.; Yao, Y.; Chenb, J. *Appl. Phys. Lett.* **2007**, *91*, 053109.
(13) Xu, Z.; Zheng, Q.; Chen, G. *Appl. Phys. Lett.* **2007**, *91*, 223115.
(14) Areshkin, D. A.; White, C. T. *Nano Lett.* **2007**, *7*, 3253.
(15) Muñoz-Rojas, F.; Jacob, D.; Fernández-Rossier, J.; Palacios, J. J. *Phys. Rev. B* **2006**, *74*, 195417.
(16) Datta, S. *Electronic Transport in Mesoscopic System*, Cambridge, 1995.
(17) Saito, R.; Dresselhaus, G.; Dresselhaus, M. *Physical Properties of Carbon Nanotubes*, Imperial College Press: London, 1998.
(18) Son, Y.; Cohen, M. L.; Louie, S. G. *Phys. Rev. Lett.* **2006**, *97*, 216803.
(19) A simplified model for generic metal electrodes[20] to get the broadening at Dirac point around 0.2 eV is used in this simulation in order to investigate the essential difference between metal contact and graphene sheet contacts based on the density of states point of view. Note that the performance of GNR SBFETs strongly depends on the interface between the metal and GNR which affects the Schottky barrier height, lattice mismatch, atomic interactions, etc.[20,24] However, in this work for the case of the generic metal, we try to give a qualitative understanding on the behavior of a contact with constant density of states, rather than quantitative comparisons between devices with normal metal and the rest of the contacts.
(20) Guo, J. Ph.D. Thesis, Purdue University, 2005.
(21) Muñoz-Rojas, F.; Fernández-Rossier, J.; Brey, L.; Palacios, J. J. *Phys. Rev. B* **2008**, *77*, 045301.
(22) In this work, LDOS(x,E) is meant to be density of states of each unit cell along transport direction while DOS(E) is meant to be the total density of states of the devices, i.e., $DOS(E) = \int_{device} LDOS(x,E)dx$.
(23) Liang, G.-C.; Neophytos, N.; Lundstrom, M.; Nikonov, D. *Journal of Computational Electronics*, accepted.
(24) Özyilmaz, B.; Jarillo-Herrero, P.; Efetov, D.; Abanin, D. A.; Levitov, L. S.; Kim, P. *Phys. Rev. Lett.* **2007**, *99*, 166804.
(25) Radosavljevic, M.; Appenzeller, J.; Avouris, Ph. *Appl. Phys. Lett.* **2004**, *84* (18), 3693.
(26) Chen, Z.; Appenzeller, J.; Knoch, J.; Lin, Y.; Avouris, Ph. *Nano Lett.* **2005**, *5*, 1497.
(27) Guo, J.; Lundstrom, M. *IEEE Trans. Electron Devices* **2002**, *49*, 1897.
(28) Özyilmaz, B.; Jarillo-Herrero, P.; Efetov, D.; Kim, P. *Appl. Phys. Lett.* **2007**, *91*, 192107.

NL080255R